Tidally-Driven Transport in Accretion Disks in Close Binary Systems

John M. Blondin [1]

Department of Physics, North Carolina State University, Raleigh NC

The effects of binary tidal forces on transport within an accretion disk are studied with a time-dependent hydrodynamical model of a two-dimensional isothermal accretion disk. Tidal forces quickly truncate the accretion disk to radii of order half the average radius of the Roche lobe, and excite a two-armed spiral wave that remains stationary in the rotating reference frame of the binary system. We measure an effective α of order 0.1 near the outer edge of the disk in all of our models, independent of the mass ratio, Mach number, and radial density profile. However, in cold disks with high Mach number, the effective α drops rapidly with decreasing radius such that it falls below our threshold of measurement ($\sim 10^{-3}$) at a radius of only one third the tidal radius. In warmer disks where the Mach numbers remain below 20, we can measure an effective α down to radii 10 times smaller than the maximum size of the disk.

Key words: accretion disks, hydrodynamics, shock waves, novae, cataclysmic variables, binaries: close
PACS: 95.30.Lz, 97.10.Gz, 97.80.Gm, 97.80.Jp

1 Introduction

Accretion disks play a prominent role in modern astrophysics, yet we remain largely ignorant of their detailed structure and local dynamics. The importance of angular momentum transport has been understood for a long time (Shakura & Sunyaev 1973, Lynden-Bell & Pringle 1974), but for many years our understanding of disks has been built on a parameterization of some unknown transport mechanism. In recent years much progress has been made in

[1] Email: john_blondin@ncsu.edu

elucidating the role of magnetohydrodynamical turbulence in mediating angular momentum transport in accretion disks. A recent review of our current understanding of transport is given by Balbus & Hawley (1998).

In addition to local sources of transport such as MHD turbulence, global processes may also contribute to the transport of angular momentum in accretion disks. In particular, spiral shock waves can act as a local sink for angular momentum (Spruit 1987, Larson 1989). Because these waves are traveling slower than the local Keplerian velocity, they contain negative angular momentum, and any dissipation at the shock will decrease the angular momentum of the orbiting gas. While spiral waves can be produced by a variety of sources, they arise naturally in binary star systems such as X-ray binaries, cataclysmic variables, and binary proto-stars, where the gravitational pull of a binary companion creates a two-armed spiral shock wave that co-rotates with the binary system.

Such spiral waves have been observed in several numerical studies, beginning with the early work of Sawada et al. (1986) and continuing with recent attempts to model the observed spiral pattern in IP Peg (Godon et al. 1998, Armitage & Murray 1998). Despite this large body of numerical work, there has been relatively little progress in the quantitative measurement of the effective transport of spiral shocks in hydrodynamic disks. This is due in large part to the fact that it is easy to set up a hydrodynamic simulation of a Keplerian accretion disk, but it is very hard to do it accurately enough to measure the relatively small transport expected due to spiral waves. One needs high numerical accuracy, a large range in radii, and long simulations covering several orbital periods. Różyczka & Spruit (1993) ran a simulation without a tidal stream for tens of orbits. While their models did exhibit a stationary two-armed spiral pattern, the shock dissipation was not enough to keep up with the cooling in their model. As the gas in the disk cooled and the Mach number increased, the spiral shocks became weaker and eventually faded away. Savonije et al. (1994) performed careful numerical simulations to study tidal effects, making a quantitative comparison with analytic calculations of the linear response of the disk to tidal forces. They found that spiral shocks were much diminished in cold disks with Mach numbers of order 25 or higher, a feature they attributed to a mismatch between the wavelength of the tidal response of the disk and the length-scale of the driving tidal force. Godon (1997) ran relatively high resolution simulations using a markedly different numerical technique (a hybrid spectral method) and found results similar to previous authors, namely a strong two-armed spiral wave. Note that both Savonije et al. (1994) and Godon (1997) had disks that covered only a limited range in radii (4 and 5 respectively), and so could not follow the propagation of spiral waves deep into the disk.

The results of these simulations suggest that spiral waves are a robust feature

of accretion disks in binary systems, and that these spiral shocks can indeed transport mass and angular momentum through the disk. They do not, however, provide a quantitative measure of this transport. The goal of this paper is to measure an effective α due to spiral shocks excited in accretion disks by the tidal forces of a binary companion.

2 An Idealized Accretion Disk

We begin by defining an idealized theoretical model of an accretion disk that we can simulate with a standard time-dependent hydrodynamics code. Of particular concern is the treatment of the thermal structure of a disk, which is determined by a balance between local energy deposition and vertical energy transport via convection and radiative diffusion. If an adiabatic equation of state is used and no outlet is provided to remove the thermal energy, the disk will gradually heat up. This approach has been used by several authors (Sawada et al. 1986), but the increasing sound speed changes the model as the simulation evolves, and ultimately leads to hot disks with a correspondingly large scale height and small Mach number.

In order to include the thermal structure of the disk, a model must include energy transport in the vertical direction. One way to do this without including radiative diffusion and three dimensions (a difficult prospect even for the fastest computers) is to model energy loss by including an ad hoc cooling function designed to remove energy at the same rate one would expect due to thermal radiation from the disk surface. Różyczka & Spruit (1993) used this approach, specifying a local cooling rate proportional to T^4. While this approach will not necessarily produce a realistic temperature structure in the presence of shocks, it does allow the use of a realistic value of γ while keeping the temperature in the disk well below the local virial temperature. Godon (1997) avoided the issue of shock heating by assuming a polytropic equation of state, $P = K\Sigma^\gamma$, where K is a predefined constant. Savonije et al. (1994) took an intermediate approach and included an energy equation but added local cooling to maintain a polytropic equation of state.

We take a slightly different approach and assume an isothermal equation of state. This is equivalent to the polytropic equation of state in the limit that $\gamma = 1$. The assumption of an isothermal gas provides for a simpler problem, fewer parameterizations, and allows for faster computation. However, the analysis of Spruit (1987) suggests that spiral waves will not propagate for a strictly isothermal equation of state, so we may be underestimating the role of spiral shocks in this work.

An ideal, isothermal gas evolves according to the Euler equations, which can

be written in conservative form as:

$$\frac{\partial \rho}{\partial t} + \nabla \cdot (\rho \vec{u}) = 0 \tag{1}$$

$$\frac{\partial \rho \vec{u}}{\partial t} + \nabla \cdot (\rho \vec{u} \vec{u}) + \nabla P = \rho \vec{a}, \tag{2}$$

where ρ is the mass density, $\vec{u}$ is the velocity, and the pressure is given by $P = c_s^2 \rho$ with c_s being the isothermal speed of sound. In a coordinate frame Co-rotating with the binary system, the acceleration of the gas can be written as

$$\vec{a} = -\nabla \Phi - 2\vec{\Omega} \times \vec{u}$$

where the last term is the Coriolis force due to the Co-rotating coordinate system, Ω is the orbital frequency of the binary system, and the effective binary potential is given by

$$\Phi = -\frac{GM_1}{r_1} - \frac{GM_2}{r_2} - \frac{1}{2}(\vec{\Omega} \times \vec{r}_{cm})^2.$$

The last term is the centrifugal force due to the Co-rotating system, and r_1 is the distance to the accreting star, r_2 is the distance to the donor star, and r_{cm} is the distance to the center of mass of the binary system. We have normalized our model such that the unit of distance is given by the binary separation and $GM_1 = 1$. In these normalized units the orbital period is $P = 2\pi/\sqrt{1+q}$, where $q = M_2/M_1$ is the mass ratio.

We further restrict our idealized model to two dimensions by assuming no vertical motions nor variations with height in the disk. When using a cylindrical coordinate system, this is equivalent to replacing the density in the disk with a surface density, $\Sigma = 2\rho H$, and assuming a constant scale height, H(Godon 1997).

Because our objective is to measure the tidal effects on transport in an accretion disk in a binary system, we need some quantitative measure of transport through the disk. The most direct physical quantity we could measure is the mass accretion rate, given by $\dot{M} = 2\pi r \Sigma v_r$ in two dimensions. The surface density has no particular scale (we chose $\Sigma = 1$ in our flat disk models); the important parameter is really the radial velocity, v_r. However, rather than reporting the average radial velocity (as compared to, say, the sound speed), we have followed the historical convention of this subject and reported the effective value of α. Shakura & Sunyaev (1973) introduced α as a means of parameterizing some unknown form of angular momentum transport, presumably related to local turbulence in some fashion. While the transport being

measured in our models is a global phenomenon rather than a local process, we can still refer to an *effective* α that would give the same mass accretion rate in an α-disk model that we find in our simulations.

The standard α-disk theory gives the mass accretion rate in terms of α as $\dot{M} = 3\pi\alpha c_s H\Sigma$, where H is the local scale height in the disk. Using the fact that $H = Rc_s/v_\phi$ for a cold, thin disk, we find an equation for α:

$$\alpha = \frac{2}{3}\frac{v_\phi \langle v_r \rangle}{c_s^2}, \tag{3}$$

where $\langle v_r \rangle$ is a density-weighted average of the radial velocity:

$$\langle v_r \rangle = \frac{\int_0^{2\pi} \Sigma v_r d\phi}{\int_0^{2\pi} \Sigma d\phi}.$$

Thus, to measure α we need to keep track of the local radial mass flux ($v_r\Sigma$) and the local surface density.

It is important to point out that our ideal accretion disk is not expected to be in strict steady state. We have no a priori reason to expect the mass accretion rate to be independent of radius. Mass accretion in this model is driven solely by the action of spiral shock waves, whose strength will certainly depend on the radius within the disk. The propagation of these shocks will also depend on the density profile in the disk, but there is no guarantee that a combination of density profile and shock propagation exists that leads to a constant mass accretion rate. Furthermore, even if there did exist a steady-state solution, we may not, in practice, be able to evolve a simulation long enough to reach a true steady state.

3 Computational Method

Our idealized accretion disk model is evolved using a modified, isothermal version of the hydrodynamics code VH-1`http://wonka.physics.ncsu.edu/pub/VH-1`, run in two-dimensional cylindrical coordinates (r, ϕ) centered on the accreting star. This code is based on the Lagrange-remap version of the piece-wise parabolic method (Colella & Woodward 1984). The isothermal version is significantly faster than the adiabatic code because there is no need to solve an energy equation and there exists an analytic solution to the Riemann problem, avoiding a costly iterative solution as required in an adiabatic code.

There are essentially two modifications to the standard distribution of the isothermal version of VH-1: Forces to account for the rotating binary potential

and changes in the remap step to allow conservation of angular momentum. This second step is vital to any quantitative study of accretion disks, for it is the transport of angular momentum that allows accretion to take place. If a numerical method does not conserve angular momentum, accretion may result solely from, or be completely wiped out by, numerical error.

Conserving angular momentum in VH-1 is a fairly simple task. When computing the hydrodynamic evolution in the ϕ direction the radius is held constant so conserving angular momentum is equivalent to conserving ϕ momentum, which VH-1 already does. When computing the evolution in the radial direction the angular momentum in a zone is left unchanged during the Lagrangian hydrodynamic evolution. This leaves the remap step in the radial direction as the only place in the standard code where angular momentum is not conserved. Fortunately, conserving angular momentum in this step is trivial: instead of interpolating on v_ϕ and remapping ϕ momentum, one need only interpolate on rv_ϕ and remap angular momentum. Doing so will conserve the total angular momentum on the grid to within machine roundoff error (if boundaries are reflecting and forces are only radial).

An additional concern is the local diffusion of angular momentum. Even if angular momentum is conserved globally, it may diffuse across the numerical grid, producing anomalous transport. Savonije et al. (1994) modified their code to interpolate on the quantity $\Sigma r^{1/2} v_\phi$ (which is flat in a Keplerian disk with constant Σ) in order to minimize the diffusion of angular momentum. This prevented unwanted instabilities from developing in their disk, although it did not necessarily guarantee conservation of angular momentum. Fortunately, VH-1 exhibits very little diffusion of angular momentum in this problem, a feature we attribute to the higher-order interpolations used in the piece-wise parabolic method.

The Lagrange-remap method used in VH-1 allows a simple, accurate measure of the radial mass flux need to compute an effective α. Advection in VH-1 is treated in the remap step, where gas that has been evolved on a Lagrangian grid is remapped back onto a fixed Eulerian grid. For example, if the Lagrangian interface between zones 1 and 2 moves to the right during a timestep, the remap step takes the mass (and momentum) within a sub-shell defined by the original zone interface and the final Lagrangian interface and instantaneously moves it from zone 1 (where this mass was before the timestep) to zone 2 (where it has advected during the timestep). The mass flux through the Eulerian interface during the timestep is just the mass in the sub-shell that was remapped from zone 1 to zone 2. So, to compute an average mass flux, $v_r \Sigma$, we summed up all the mass being remapped across a given radial boundary (i.e., for all values of ϕ) during a prescribed interval of time (typically 50 time steps). Dividing by the average (over time and ϕ) density in these sub-shells, we can calculate an effective value of α.

The initial conditions for the disk simulations include a low-density hole in the first 5 radial zones (10^{-3} of the disk density) to act as a buffer between the inner edge of the disk and the inner boundary, zero radial velocity, and $v_\phi = r^{-1/2} - \Omega r$. The last term in v_ϕ accounts for the centrifugal force in the rotating reference frame, and provides for an initial disk much closer to equilibrium than pure Keplerian rotation.

The ϕ boundaries are periodic and the radial boundaries are constructed to allow material to flow off the grid, but not onto the grid. At the inner radial boundary the ϕ velocity is set to zero in the ghost zones (extra zones used for interpolation on the real grid), creating an imbalance of forces at the inner edge of the hydrodynamic grid that drives quick accretion off the inner edge. Contrary to some previous numerical work (Matsuda et al. 1990), the exact boundary conditions at the inner edge do not significantly alter the simulations. Even with a reflecting boundary, material piles up at the inner edge of the grid without influencing the spiral shocks at larger radii. The outer boundary also does not exert much influence on the long term evolution of the disk. Once tidal forces trim down the outer edge of the disk, the density in the outer zones is very small so there is negligible flux of mass and momentum off the outer edge of the grid.

Most of our simulations were run on grids with a radial span of a factor of 20, with the radial zone size gradually increasing with increasing radius to provide consistent resolution over the full range of radii in the simulation. The outer radius was chosen to be approximately the distance to the inner Lagrange point, allowing plenty of room between the outer edge of the tidally-truncated disk and the outer grid boundary. One would like to make the inner edge of the numerical grid as small as possible, but restrictions on the timestep in an explicit hydrodynamic code make small inner radii very expensive to compute. For stability, the timestep must be less than $r\Delta\phi/v_\phi$. But $v_\phi = r^{-1/2}$ in an accretion disk, so the limiting timestep decreases as $r^{3/2}$. Evolving a disk that extends down a factor of 20 in radius thus requires a small timestep and a corresponding large number of cycles; some of our simulations ran for over 10^6 cycles. The choice of 20 for the radial span was based on the radial decay of α in our standard model, as we will see in the following section. This inner radius also corresponds roughly to the point of closest approach for a ballistic stream of gas originating at the L_1 point in the binary system. Since our goal in future work is to quantify the effects of the tidal stream on transport within the disk, we have extended our disks in this work down to this small radius.

The issue of numerical resolution was approached empirically. Keeping in mind that our goal was a quantitative measure of transport effects caused by tidally-induced spiral waves, we ran several simulations with different numerical resolutions. We found relatively little difference in the density structure of the disk and the computed value of α when we used 115 zones in the ϕ direction

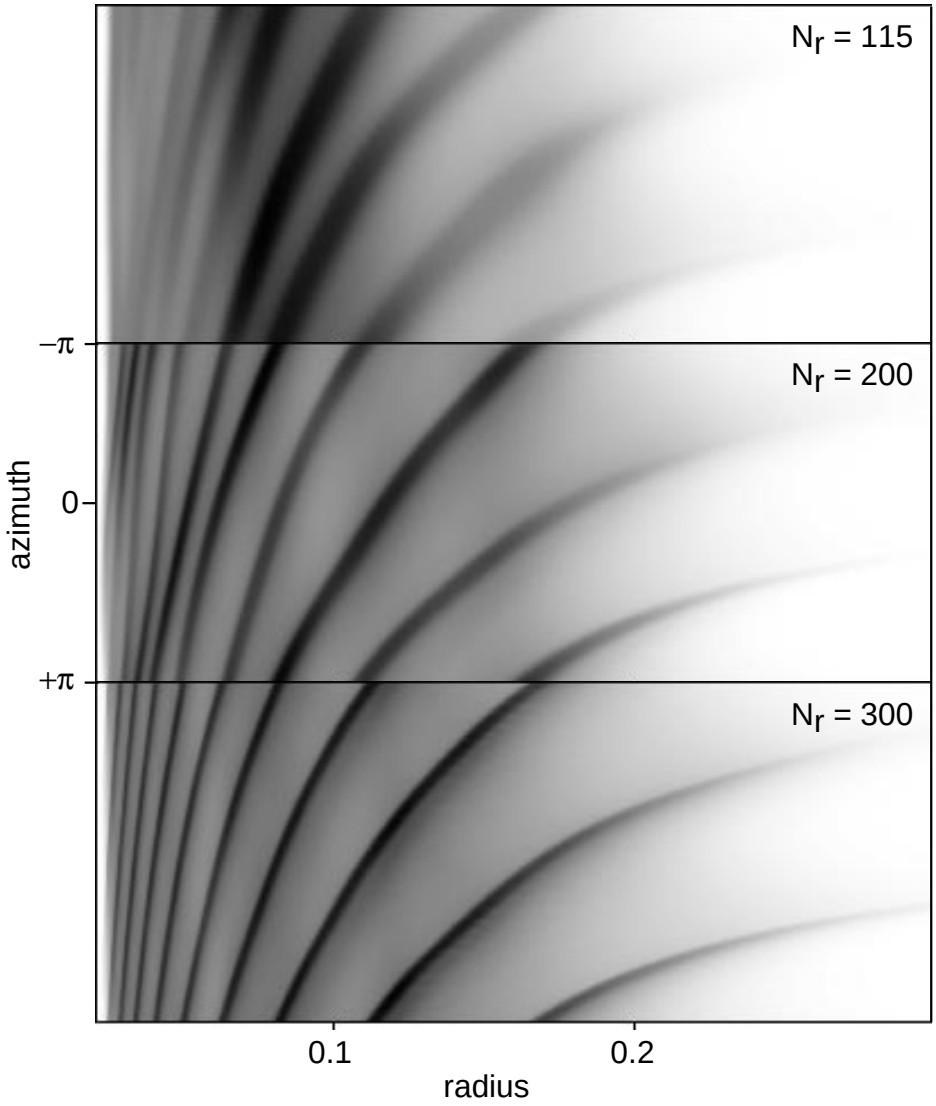

Fig. 1. Resolution of spiral waves as a function of the number of radial zones, n_r. The grey scale represents gas density, which reaches a maximum of approximately 3 times the initial disk density in the spiral waves.

compared with 200 zones, so we opted for the former in most simulations. For the radial direction we found significant differences between runs with 115 and 200 radial zones, but relatively little difference between runs with 200 and 300 radial zones. Figure 1 shows the loss of definition in the spiral waves when the radial resolution is too low. The computed value of α in the run with 200 zones evolved very similar to that in the run with 300 zones, but the run with 100 zones looked completely different (and in fact was negative throughout the evolution). More radial zones were required for the colder disk simulations described in Section 4.2

Finally, a small amount of dissipation was included in the code in the form of wiggling the grid back and forth a small amount in the radial direction (Colella

& Woodward 1984). This was necessary in order to suppress two different numerical instabilities found in these disk simulations. The first creates a zone to zone striping in the radial direction, and the second leads to epicyclic waves, usually (but not always) appearing at the inner boundary of the disk. The first problem is related to the conservation of angular momentum. In a one-dimensional (radial) problem using Lagrangian coordinates, if a given zone has too much angular momentum it will drift outwards. However, this motion will drag out neighboring zones, which will find themselves having too little angular momentum for their new radius and will drift inwards. This can lead to a striping effect with the radial velocity in each zone changing sign from zone to zone. We were not able to fully understand the second problem, but we found that it was worse (in the absence of grid wiggling) if the ratio of the sound crossing time across a radial zone to the orbital period at that radius was larger than some critical value. For all practical purposes these instabilities were eliminated by the grid wiggling, which in turn had negligible effect on the structure of the disk or the computed value of α.

As a test of our computational method we ran a simulation without the binary potential, i.e., with only the central force of the accreting star's gravity. We instituted reflecting boundary conditions at both the inner and outer radii, so the total mass and angular momentum on the grid should remain fixed. To make the test meaningful, we perturbed v_ϕ in a small band of radii in the middle of the grid to create wave motions. The mass and angular momentum did remain constant to within machine round off error. The local radial velocities remained less than $\sim 10\%$ of the sound speed, and the computed average of α was $\sim 10^{-3}$. This then represents the limit to which we can measure an effective α in our binary simulations.

4 Numerical Simulations

This section describes seven hydrodynamic simulations varying the sound speed, mass ratio, and density profile in the disk. The parameters describing each of these models are listed in Table 1.

4.1 Standard Model

For the purposes of presenting our results we have adopted a standard model in which $q = 1$ and $c_s = 0.25$. We will describe this model in detail, and then go on to discuss how other models differ from this standard. With the adopted sound speed, the Mach number of the disk material at the inner edge of the disk is ~ 28, comparable to some of the best previous numerical work, but still

Table 1
Input parameters (sound speed c_s, mass ratio q, and surface density index n) for the hydrodynamic simulations. The tidal radius, R_T, and the Mach number of the Keplerian flow at half the tidal radius are given, as well as the ratio of the tidal radius to the radius of the Roche lobe of the accreting star.

Model	c_s	q	n	R_T	R_T/R_L	$M(R_T/2)$
standard	0.25	1.0	0	.214	0.56	12.2
colder	0.125	1.0	0	.264	0.69	22.0
coldest	0.0625	1.0	0	.300	0.79	41.3
steeper	0.25	1.0	1	*	*	12.2
steepest	0.25	1.0	3	*	*	12.2
lowmass	0.25	0.2	0	.307	0.59	10.2
highmass	0.25	5.0	0	.185	0.74	13.2

lower than one might expect in real disks. Tidal forces quickly truncate the disk at an outer radius of 0.21, which is roughly half of the averaged Roche lobe radius as given by the analytic expression of Eggleton (1983). This disk is significantly smaller than predicted by theoretical arguments for infinitely cold disks(Paczynski 1977), but one expects that finite pressure effects will increase the effectiveness of tidal forces in truncating the disk. At this tidally-truncated outer edge the disk material orbits with a Mach number of ~ 8.

The images and associated animations in Figure 2 show the strong spiral structure that develops in our standard model. The two-armed spiral wave remains relatively fixed in the co-rotating reference frame of the hydrodynamic simulation. The shape of the spiral is determined by the inward radial propagation of the wave at a velocity of order the sound speed and the shearing of this wave by the orbital motion. The result is a trailing angle (between the spiral shock and a circle of given radius) given by $\tan\Theta \approx (c_s/\Omega r)$ (Godon et al. 1998), or the inverse of the Mach number of the orbital motion, M. Larson (1989) suggested a radial wave speed of $\sim 1.5c_s$, whereas our simulations show a spiral shape corresponding to a wave speed of $\sim 1.3c_s$. The density jump at the spiral shocks varies from a maximum of ~ 2.1 near the outer edge of the disk down to a value of ~ 1.4 near the inner edge. The corresponding shock Mach numbers of order ~ 1.3 (given by the square root of the compression) are in agreement with the low Mach numbers predicted by Spruit (1987) and with the predicted shape of the spiral pattern. Presumably the strength of the spiral shocks would continue to decrease if we had extended our simulation down to even smaller radii, as the spiral shock becomes wound tighter and tighter with increasing orbital velocity.

The initial response of the disk to the binary potential and the subsequent

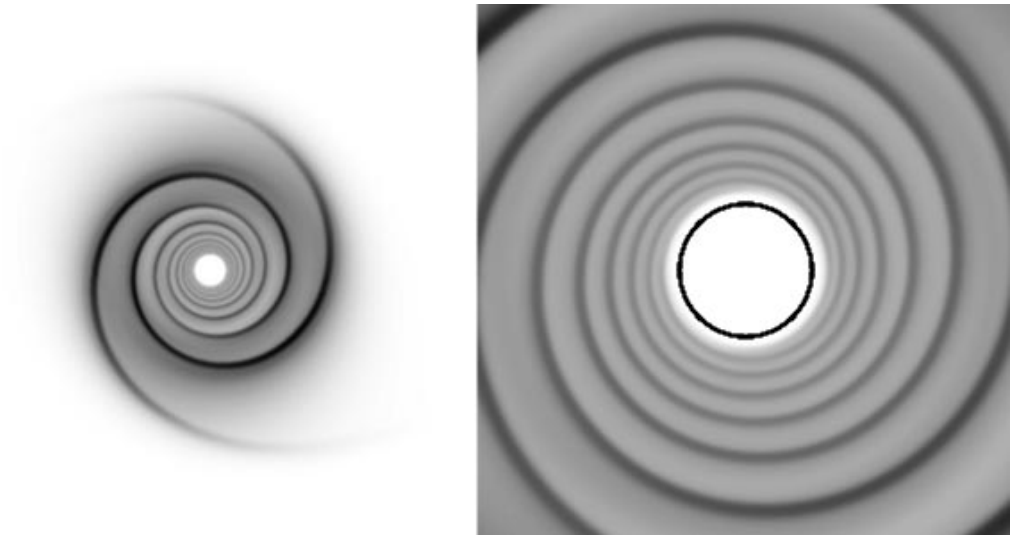

Fig. 2. Density in the standard model at time $t = 9$. The left image shows the entire grid spanning the Roche lobe of the accreting star, while the right image shows the central region magnified by a factor of 5. The binary companion is to the right of the image,and the disk orbits in a clockwise sense. Black corresponds to high density gas, with saturation occurring at a density of 3. The black circle in the right image marks the inner edge of the numerical grid at $r = 0.02$. The accompanying animations show the evolution of the disk from the same two perspectives.

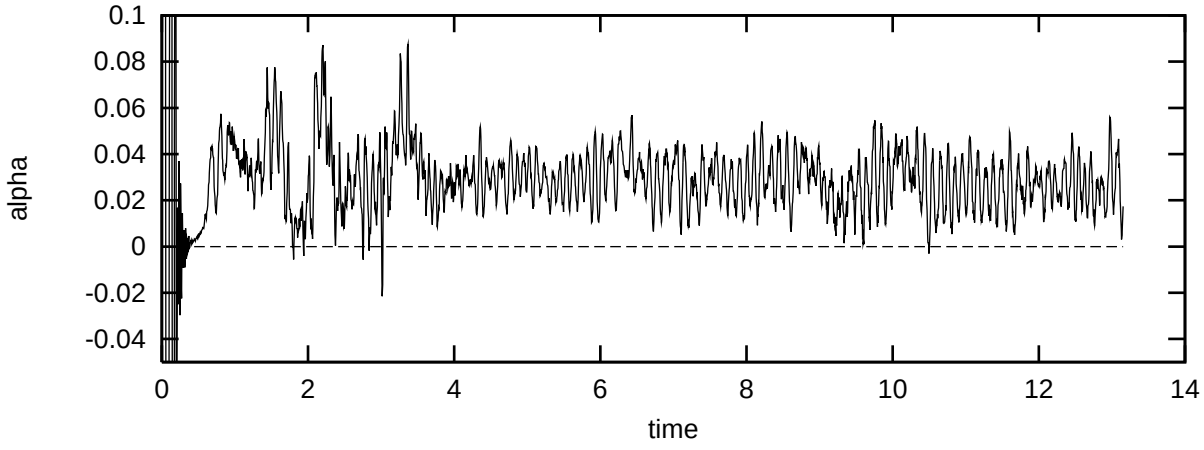

Fig. 3. Time evolution of α in the standard model at a radius of $r = 0.065$. The Keplerian period at this radius is $P_{kep} \approx 0.105$.

quasi-steady transport are illustrated in Figure 3, which plots the effective α at a radius of $r \approx 0.065$. There are very large waves generated by our crude initial conditions, as shown by the large variations in α shortly after $t = 0$, but these quickly dissappear on a timescale of less than one rotation of the outer disk edge. The behavior of α does not appear to settle into a quasi-steady behavior until after approximately one orbital period (4.44 in this model), but from 1 to 3 orbital periods the behavior appears unchanged.

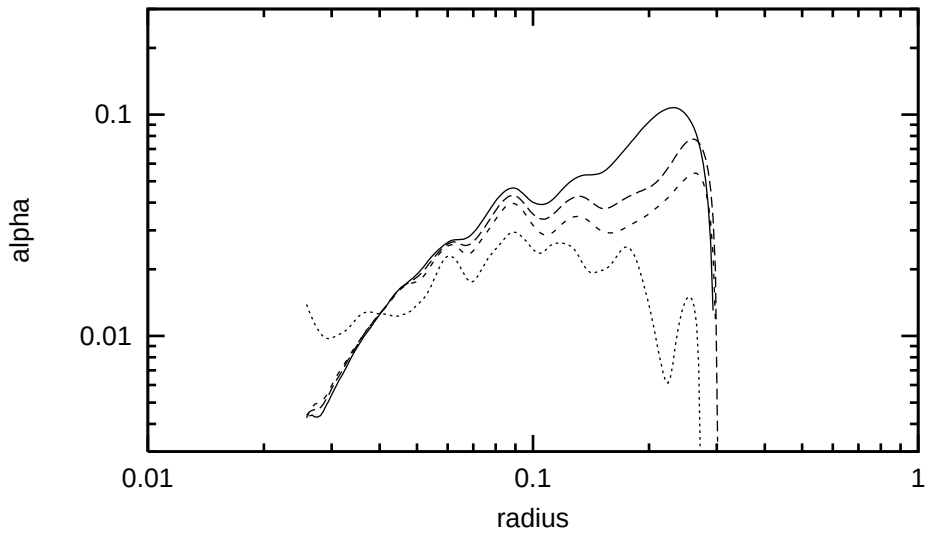

Fig. 4. Time-averaged radial profile of α in the standard model for times of 7-9 (solid), 9-11 (long dash), and 11-13 (short dash). The dotted line shows α at late times ($t = 25 - 27$) after other wave modes have appeared in the outer regions of the disk.

The high frequency oscillations clearly visible in Figure 3 correspond to the local Keplerian frequency ($P_{kep} = 2\pi r^{3/2} \approx 0.105$).

The variation of α with radius is shown in Figure 4. The value of α is as high as 0.1 near the outer edge of the disk where strong spiral shocks are driven by tidal forces, but appears to gradually decline with time at large radii. Inside of $r \approx 0.1$, α appears relatively constant with time but drops with decreasing radius. Although $\alpha(r)$ is not well fit by a power-law, we can approximate α in the central region of the disk with $\alpha \approx r^{1.4}$. At late times other wave modes appear (see the animation in Fig. 2), slightly reducing α at large radii and enhancing it at small radii. The result is a more uniform value of α throughout the disk. However, more analysis of these other wave modes is needed before one can be confident of their role in angular momentum transport. For this reason we concentrate our attention on the two-armed spiral waves.

These values of α due to the two-armed spiral shocks are consistent with the shock strengths quoted above, but the radial dependence is much steeper than the predictions of Larson (1989), and the absolute values are much higher than the analytic predictions. For a spiral shock with Mach number M_s, Larson (1989) derives an effective α in an isothermal disk of

$$\alpha \approx 0.07(M_s^2 - 1)^3 \,. \tag{4}$$

For an isothermal shock, M_s^2 is equal to the compression ratio. The range in M_s^2 from 1.4 to 2.15 gives a range in α of 0.005 to 0.1, consistent with the

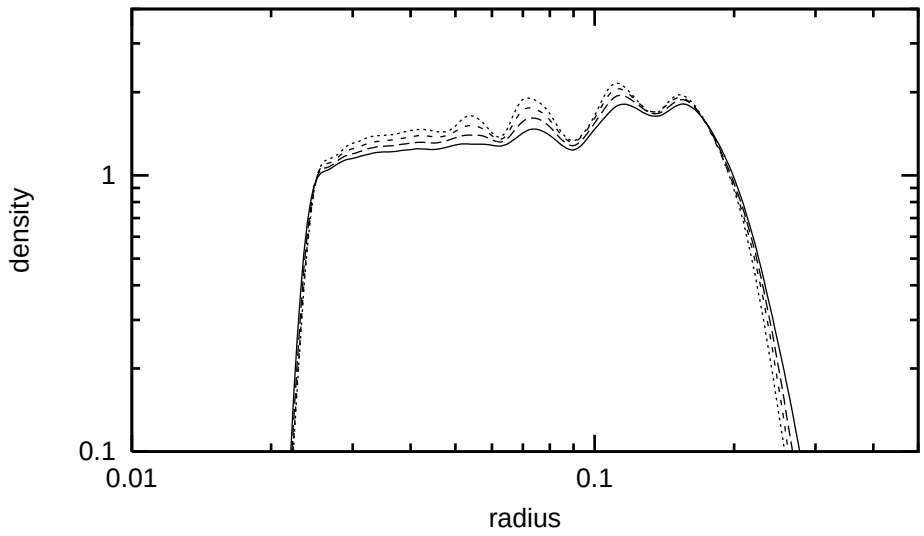

Fig. 5. Radial profile of Σ (averaged over ϕ) in the standard model at various times beginning with $t = 9$ (solid line) and ending with $t = 16$ (dotted line).

data plotted in Figure 4.

Larson (1989) goes on to predict that the strength of tightly wound spiral shocks in a cold, thin disk should be proportional to $(\cos\theta)^{3/2}$, where θ is the trailing angle of the spiral wave. Estimating $\cos\theta \approx 1.5 c_s/v_o$, Larson (1989) finds an effective α of

$$\alpha \approx 0.026 \left(\frac{c_s}{v_o}\right)^{3/2} . \tag{5}$$

The prediction for an isothermal disk with $c_s = 0.25$ is $\alpha \approx 3.2 \times 10^{-3}\, r^{3/4}$, orders of magnitude below that found in our simulations.

A simple estimate of the timescale for gas to move through the disk is r/v_r, which for this model ranges from 60 at the outer edge of the disk to ~ 300 near the inner edge. Having evolved our simulation for a time of only 13, we do not expect our model to have settled into an equilibrium. We can in fact see small changes in the density profile of the disk as plotted in Figure 5. Despite the fact that the density is slowly increasing over most of the disk, the total mass on the computational grid has decreased by almost 1% during the time from $t = 9$ to $t = 16$.

The two-armed spiral pattern seen in Figure 2 is not the only wave present in the disk. On a timescale of several binary orbits other wave modes begin to appear. By viewing the animation accompanying Figure 2, one can identify a purely radial wave ($m = 0$) and a precessing eccentric wave ($m = 1$) growing in the vicinity of the outer disk edge. While these waves continue to grow to

some apparent saturation level, they do not completely disrupt the two-armed spiral shock, and α remains at a significant level 4. Similar wave modes have been seen in the simulations by Godon (1997). We will discuss them further in the next section, for they are more apparent in colder disks.

4.2 Dependence on Mach Number

The sound speed in our standard model was chosen to produce a significant value of α, not because it was astrophysically interesting. In most accretion-powered binary systems the Mach number of the orbital motion in the disk will be much higher than we have assumed here. A colder disk is both more challenging to simulate and more difficult to measure the expected smaller α. The effect of spiral shocks on transport through an accretion disk diminishes rapidly with increasing Mach number because the spiral shocks are wound tighter, making the relative shock Mach number smaller, leading to less dissipation and effective transport.

In addition to the challenge of measuring small effects, we were faced with several numerical problems when simulating colder disks. The first problem is one of resolution. Because the spiral arms are wound tighter in colder disks, we found that to accurately resolve the oblique shocks of the spiral arms, we needed higher resolution in the radial direction. Another difficulty plaguing our cold disk simulations was the increase in numerical "noise" with higher Mach number. In one-dimensional (radial) simulations of Keplerian disks excited with radial waves, we found a monotonic increase in the average radial velocity with increasing Mach number in the disk. While the effective α from this numerical noise remained low ($\alpha = 4 \times 10^{-3}$ for $c_s = .0125$), it could affect the measurement of transport in very cold disks. Finally, the numerical instabilities described in the appendix are more apparent at higher Mach numbers.

To investigate the influence of sound speed on our idealized accretion disks we ran simulations similar to our standard model but with sound speeds of 0.125 (with 300 radial zones) and 0.0625 (with 400 radial zones). As expected, the tidal forces have less of an effect on the colder disks. As seen in Figure 6, the spiral density waves are wound tighter and fade faster with decreasing radii in the colder, higher Mach number disks. The two-armed spiral has almost completely disappeared by the inner edge of the disk with $c_s = 0.125$, and is present only beyond $r \approx 0.08$ in the coldest disk.

A one-armed spiral is clearly visible in the interior of the coldest disk. This wave originates in the outer regions of the disk and propagates inward, decaying away below a radius of $r \approx .04$. There is no trace of this wave at the inner edge of the disk at any time during the simulation. A similar wave can be seen

in most of the other simulations, showing up either as an initial transient, or as a growing mode at late times in the simulation. However, this wave is much harder to identify in the other models, both because the single spiral is weaker, and also because the double spiral is much stronger in warmer disks and hence obscures the single spiral. The one-armed spiral is easily seen in the animation of the cold disk with $c_s = .125$, but it is a transient phenomena, presumably excited by the initial conditions. At later times there is a faint hint of the one-armed spiral, but it is much weaker than the double spiral wave.

The source of this single spiral wave (ignoring for the moment any transient created by the initial conditions) may be related to the fact that the double spiral wave at the outer edge of the disk is not steady, and in fact is much less steady in the coldest disk where the single spiral is most prevalent. In contrast to the standard model, there appears to be at least two competing waves excited at the tidal radius in the coldest disk model, for the two-armed spiral is never steady.

Godon (1997) also observed a single spiral in his Model 1, which has Mach numbers comparable to our coldest disk. He attributed this wave to "viscous oscillations" excited by the tidal potential. In contrast to our simulations however, Godon (1997) found that the single spiral wave was trapped between the reflecting inner boundary and the outer edge of the disk. As a consequence, this wave grew unbounded in his simulation and eventually dominated the entire disk. In addition, the presence of this wave was closely tied to his choice of a Keplerian, reflecting inner boundary. Any deviation from this assumption and the single spiral did not appear. In our simulations, which covered a radial range four times larger, the single spiral decayed away before reaching the inner edge of the disk, and its presence was unaffected by the choice of inner boundary conditions.

These simulations also provide evidence that tidal truncation becomes less effective with increasing Mach number. The tidal radius of the coldest disk is $\sim 80\%$ of the averaged Roche lobe radius, more in line with the analytic predictions of Paczynski (1977). By searching for the largest non-intersecting periodic orbits, Paczynski (1977) found an upper limit (in the absence of pressure effects) to the size of an accretion disk. For a mass ratio of unity, he predicted a maximum disk radius of 0.3, in good agreement with the tidal radius in our coldest model. The warmest model had a tidal radius of 0.214, some 30% smaller, leaving the disk radius only 60% of the Roche lobe radius.

Figure 7 shows the precipitous drop in α as a function of radius for cold disks. Analytic arguments suggest that α should drop as $c_s^{3/2}$, but maintain the same $r^{3/4}$ radial dependence in an isothermal disk. We find that the maximum value of α, found near the outer edge of the disk, remains roughly independent of

Fig. 6. Snapshots of the disk surface density in models with a sound speed of $c_s = 0.25$ (left), 0.125 (center), 0.0625 (right). The accompanying animations illustrate the increasingly unsteady behavior as the sound speed is reduced.

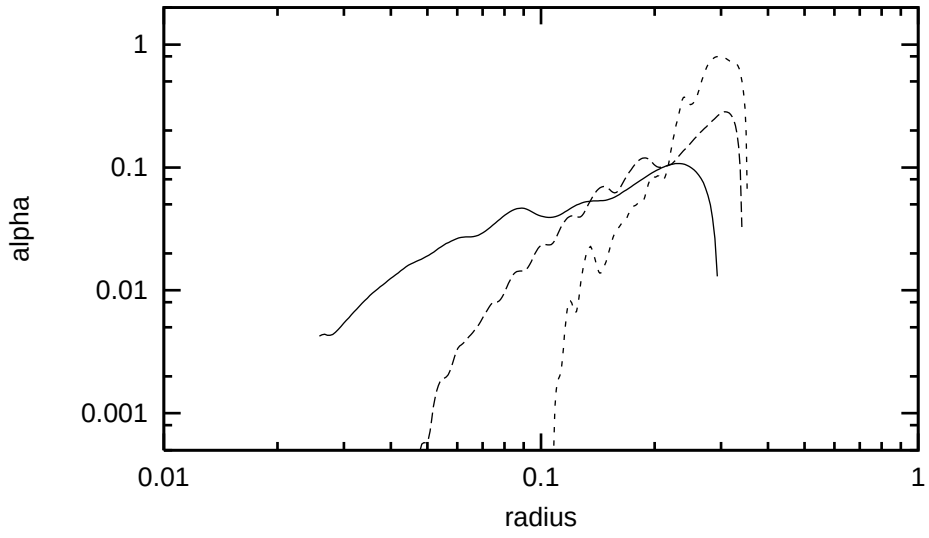

Fig. 7. Dependence of the effective α on the sound speed in the disk. The solid line corresponds to the standard model with $c_s = 0.25$, the long-dashed line to the model with $c_s = 0.125$, and the short-dashed line to the model with $c_s = 0.0625$.

sound speed, while the radial dependence of $\alpha(r)$ steepens with decreasing sound speed. In fact, because the radial decay of α is so steep, we found steady mass accretion only for radii above $r \approx 0.1$ in the coldest disk with an outer Mach number of ~ 32.

4.3 Dependence on Density Profile

The results of our models so far are characterized by a relatively steady mass accretion rate that varies with radius in the disk. This implies that the density

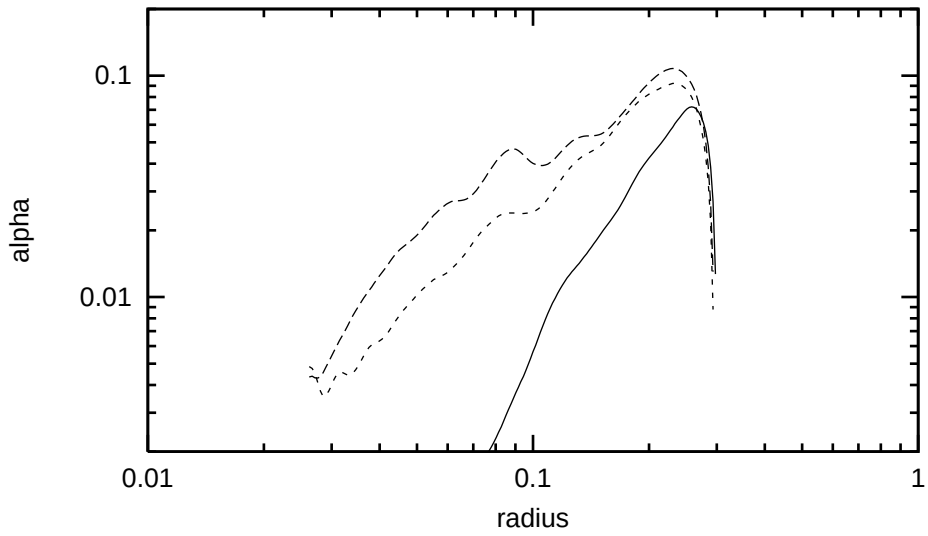

Fig. 8. Dependence of the effective α on the density profile in the disk. The solid line corresponds to the model with $n = 3$, the short-dashed line to the model with $n = 1$, and the short-dashed line to the standard model with $n = 0$.

profile is changing with time as mass piles up in the disk. Left to evolve for a much longer time, we would expect the density profile to steepen, with higher densities at smaller radii where the spiral waves are less effective at transporting angular momentum. Would this different density profile affect the computed value of α in the model? Will the spiral waves weaken as they propagate down into regions of higher density?

We ran additional simulations for several density profiles $\Sigma \propto r^{-n}$, and show results for $n = 0$, 1, and 3 in Figure 8. For comparison, an α-disk model for an isothermal equation of state yields $n = 1.5$, and for an adiabatic gas $n = 0.75$ (Shakura & Sunyaev 1973). Note however that the gas density scales with a steeper function of radius than the surface density. In a three-dimensional isothermal model the scale height increases as $H \propto r^{3/2}$, so the density in the equatorial plane varies as $\rho \propto r^{-3}$.

In all but the most extreme model, the effective transport within the disk is very similar. The value of α is down by at most a factor of ~ 2 in the inner disk for the model with $n = 1$ as compared to the standard model, but the radial dependence, maximum values, and tidal truncation all appear similar in the models with $0 < n < 1.5$. In contrast, the spiral waves decay much faster in the steepest disk with $n = 3$. The spiral waves still extend all the way to the inner edge of the disk in this model, but the radial velocity perturbations and density compressions associated with these waves are lower than found in the other models with smaller n. As a consequence of this faster decay, the mass accretion rate is still an increasing function with radius, despite the fact that the density varies as $\Sigma \propto r^{-3}$. This result suggests that a true steady

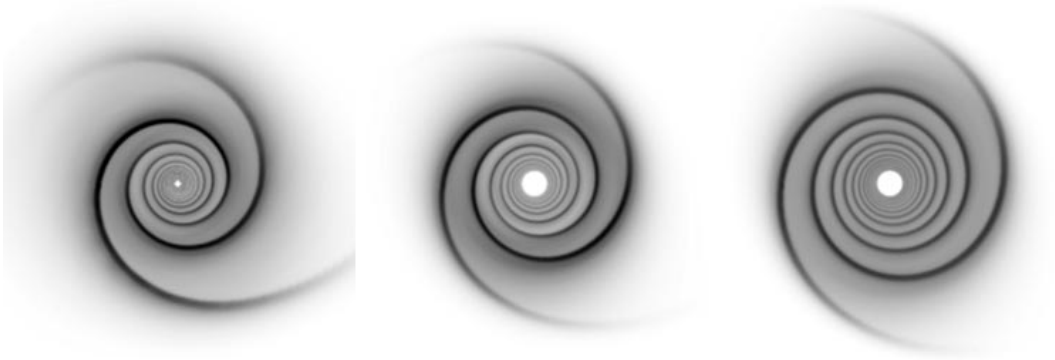

Fig. 9. Effect of mass ratio, q, on the spiral pattern, with $q = 0.2$ on the left, $q = 1$ in the center, and $q = 5$ on the right. Each image has been scaled to the size of the Roche lobe. The $q = 0.2$ model was evolved on a grid that went down to much smaller radii. The density scale in each image has been normalized to the average density in the middle of the disk.

state may not exist for a two-dimensional isothermal accretion disk in which transport is mediated solely by tidally-induced spiral shocks.

4.4 Dependence on Mass Ratio

Our last parameterization is the mass ratio, q. In addition to the equal mass system studied in the previous subsections, we have run simulations with a mass ratio smaller than unity (accretion *from* a lower mass companion) and larger than unity (accretion *from* a higher mass companion). The spiral patterns shown in Figure 9 are remarkably similar for different values of q. The spiral waves are slightly more open for small q. Since the disk extends out to larger radii where the Keplerian velocity is smaller, the Mach number is lower and the trailing angle of the spiral is larger. The strength of spiral shocks, as measured by the shock compression, is comparable in all three simulations.

The relative independence of our model on the mass ratio (at least within the limited range that we have simulated) is also seen in Figure 10, which shows an effective α that does not vary much with q. The only significant difference is the location of the outer edge of the disk. But when the tidal truncation radius is compared with the radius of the Roche lobe (Eggleton 1983), R_L, even the size of the disk does not change much. Accretion from a low-mass companion produces a larger disk, but the Roche lobe is larger by almost the same amount, leading to a ratio of R_T/R_L comparable to a disk in a binary with equal mass stars. Accretion from a high-mass companion produces a smaller disk, but one that occupies a larger fraction of the Roche lobe (Table 1).

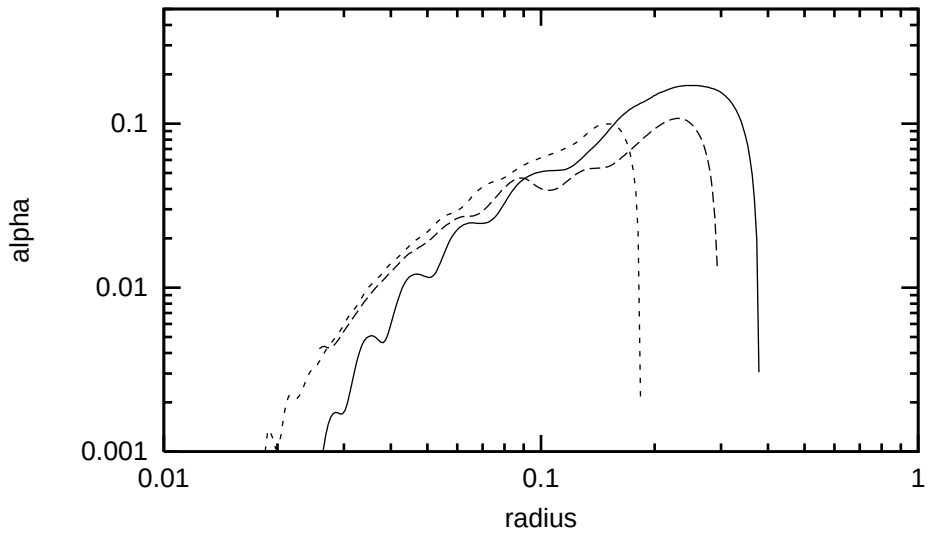

Fig. 10. Dependence of the effective α on the mass ratio, q. The solid line corresponds to $q = 0.2$, the long-dashed line to the standard model with $q = 1$, and the short-dashed line to $q = 5$.

5 Discussion

The time-dependent hydrodynamic simulations presented in this paper clearly show that, within the limitations of the idealized model, tidally-induced spiral shocks can lead to significant radial transport in accretion disks in binary systems. Our results agree qualitatively with previous numerical work; namely, we find that tidal forces excite a two-armed spiral shock wave that remains stationary in the rotating frame of the binary system. However, our use of high spatial resolution and a high-order numerical algorithm that conserves angular momentum about the accreting star allows us to quantitatively measure the transport effects of these spiral waves.

Perhaps the most interesting result is that α is large. In all of our simulations, the effective α was at least 0.1 in the outer regions of the accretion disk where the tidal shock waves are excited. However, as predicted by analytic arguments, α decays with decreasing radius. In cold disks such as those found in CV systems, this drop is so precipitous that we could not measure an α below a radius of only 1/3 that of the outer edge of the disk.

These numerical results agree in many respects with the analytic work of Larson (1989) and Spruit (1987). The shape of the spiral wave agrees reasonably well with the simple prediction that the trailing angle should be roughly the inverse of the orbital Mach number (Godon 1997), and the Mach number of the spiral shocks matches the values found in the self-similar models of Spruit (1987). Even the value of the effective α in terms of the Mach number of the

spiral shocks, M_s, agrees with the analytic estimate of Larson (1989).

However, the value of the effective α in our simulations is much larger than the analytic predictions of Larson (1989) and Spruit (1987) when written in terms of the orbital Mach number of the disk. In addition, the dependence of α on sound speed and disk radius does not agree with their analytic theory, which predicts an effective α proportional to $(c_s^2 r)^{3/4}$. This discrepancy thus appears to lie in the derivation of the Mach number of the spiral shock as a function of the sound speed in the disk.

We note, however, that the analytic work applies to the propagation of spiral waves through a disk, and does not give reference to the source of the waves. This work shows that tidal forces drive a strong two-armed spiral wave, which in turn produces an effective $\alpha \approx 0.1$ in the outer regions of the disk. As this wave propagates inward, there is a competition between growth and dissipation, as well as the effects of an increasing Mach number. In our models dissipation wins out and the wave weakens (as measured by radial velocity, density compression, or effective α) as it propagates to smaller radii. Perhaps it would eventually approach the analytic solution as it continues to weaken, but the corresponding α of such a wave is much smaller than we would be able to measure.

A further result of these simulations is the relative independence of spiral waves on the mass ratio in the binary system. The strength of the two-armed spiral shocks at their origin near the outer edge of the disk was fairly constant in all of our models. This has the consequence that, despite all else, one can be confident that the effective α in the outer regions of an accretion disk in a binary system is (at least) ~ 0.1.

Finally, these models allow us to investigate the effects of tidal truncation. We found a strong dependence of the tidal radius on the Mach number in the disk, such that colder disks extended out to larger radii. The tidal radius in our coldest model (with $q = 1$) agrees well with the analysis of Paczynski (1977), who found the largest non-intersecting periodic orbit in a pressure-less disk. Our results suggest that pressure effects in a warm disk can significantly decrease the tidal radius (30% smaller for a Mach number of ~ 10 at the outer edge of the disk).

There are three important caveats concerning our idealized model of an accretion disk. The first is our assumption of an isothermal equation of state. Internal heating in a real accretion disk will lead to a sound speed that increases with decreasing radii. Spiral waves in such a disk will not be as hampered by the rapid increase in Mach number that we found in our simulations, so we might expect the transport due to such waves to be significant deeper into the disk. A real equation of state (with $\gamma > 1$) is also expected to produce stronger

transport effects (Spruit 1987). Our second major assumption is the limitation to two dimensions. In general, one might expect the inclusion of the third dimension to result in weaker spiral waves in the equatorial plane, since the vertical direction provides for the possibility of additional wave modes, vertical expansion that may diminish the effects of shock compression, or refraction of waves out of the equatorial plane.

The third caveat is the missing tidal stream in our model. We found the most important effects of the spiral shocks to occur at the outer edge of the accretion disk, yet for a steady-state accretion disk there must be some source of incoming gas. In a close binary system this is most likely a tidal stream originating at the inner Lagrange point of the binary potential. This stream will presumably strike the outer edge of the disk and drive its own spiral wave into the disk (Shu 1976). Will this impact wave transport angular momentum? Will it interfere with the tidally-driven spiral waves?

While there is still a great deal of work to be done, it is clear from this and previous work that tidally-driven spiral waves can effectively drive mass transport through the outer regions of an accretion disk in a close binary system.

Acknowledgement

This research was supported in part by an NSF Career grant and a Cottrell Scholars Award from the Research Corporation. The numerical simulations described in this paper were computed on a Cray T916 at the North Carolina Supercomputing Center.

References

Armitage, P. J. & Murray, J. R. 1998, MNRAS, 297, L81. (1998MNRAS.297L..81A)

Balbus, S. A. & Hawley, J. F. 1998, Rev. Mod. Phys., 70, 1.

Colella, P. & Woodward, P. R. 1984, J. Comput. Phys., 54, 174.

Eggleton, P. P. 1983, ApJ, 268, 368. (1983ApJ...268..368E)

Godon, P. 1997, ApJ, 480, 329. (1997ApJ...480..329G)

Godon, P., Livio, M., & Lubow, S. 1998, MNRAS, 295, L11. (1998MNRAS.295L..11G)

Larson, R. B. 1989, in The Formation and Evolution of Planetary Systems, eds. H. A. Weaver & L. Danly (Cambridge:CUP), 31.

Lynden-Bell, D. & Pringle, J. E. 1974, MNRAS, 168, 603. (1974MNRAS.168..603L)

Matsuda, T., Sekino, N., Shima, E., Sawada, K., & Spruit, H. 1990, A&A, 235, 211. (1990AA....235..211M)

Paczynski, B. 1977, ApJ, 216, 822. (1977ApJ...216..822P)

Różyczka, M. & Spruit, H. C. 1993, ApJ, 417, 677. (1993ApJ...417..677R)

Sawada, K., Matsuda, T. & Hachisu, I. 1986, MNRAS, 219, 75. (1986MNRAS.219...75S)

Savonije, G. J., Papaloizou, J. C. B., & Lin, D. N. C. 1994, MNRAS, 268, 13. (1994MNRAS.268...13S)

Shakura, N. I. & Sunyaev, R. A. 1973, A&A, 24, 337. (1973ApJ....24..337S)

Shu, F. 1976, in Structure and Evolution of Close Binary Systems, ed. P. Eggleton et al. (Dordrecht: Reidel).

Spruit, H. C. 1987, A&A, 184, 173. (1987AA....184..173S)